Underestimated charge storage capability in carbon cathode for advanced alkali-metal ion capacitors

Received 00th January 20xx,
Accepted 00th January 20xx

DOI: 10.1039/x0xx00000x

Hong Tan,[a] Xiuyi Lin,[a] Jianqiu Huang,[a] Jiaqiang Huang,[a] Maijia Shi,[a] Xiaoqiong Du [a] and Biao Zhang *[a,b]

Li-ion capacitors (LICs) are emerged as complementary energy storage devices to Li-ion batteries to satisfy some specific application where high power density and long cycle life are required. The wide usage of LICs necessitates a promising energy density, which is the main challenge at this stage. In this work, we increase the energy density of LICs via both the material optimization and charge storage mechanism exploration. Porous carbon with a high surface area of over 2800 $m^2 \cdot g^{-1}$ was fabricated from alkali lignin through a traditional KOH activation method assisted by self-activation. A wide voltage window of 1.0-4.8 V is applied where synergistic storage of anions and cations is achieved. It shows that a deep discharge down to 1.0 V is necessary for full desorption of anions which also triggers the adsorption of cations (Li^+), resulting in an increased capacity. However, a compromise must be made on the energy efficiency due to the intensified battery polarization upon deep discharging. Furthermore, the Na- and K- ion capacitors are also investigated using the as-prepared carbon materials considering the natural abundance of sodium and potassium over lithium for sustainable development.

1. Introduction

Efficient utilization of clean energy has long been afflicted by the unsatisfied performance of power sources. Li-ion batteries (LIBs) have been the primary choices originating from their enormous success in portable electronics. The extension to stationary energy storage and electric vehicles is haunted partly by the limited power densities and depleted precious metal sources such as cobalt. Li-ion capacitors (LICs) are designed to meet these challenges.[1,2] Porous carbon materials and their hybrids with oxides/nitrides are adopted as cathodes to avoid the utilization of costly and toxic metals.[3-5] In contrast to Li ion intercalation in LIBs, the primary charge storage mechanism in the cathode side of LICs relies on the anion adsorption. The capacitive behaviour possesses much faster kinetics than the faradaic reaction in batteries, which bestows higher power densities on LICs to complement LIBs in application fields such as regenerative braking for trains.

A great number of precursors has been utilized to prepare the porous carbon, including polymers, graphite, pitch and biomass.[6,7] Among these, biomass precursors have received considerable attention recently due to not only its natural abundance but also the beneficial effect on the environment. Municipal solid waste becomes a big problem in the modern city, where biomass waste occupies a great portion. To turn the waste into treasure, designing an effective strategy to produce carbon materials from biomass is highly desired. Biomass is mainly consisted of lignin, cellulose and hemicellulose, with lignin being the most attractive because of its highest carbon yield of around 60%. For application in LICs, the surface area of lignin-derived carbon is increased by several approaches such as template guided and activation induced.[8] A super-high surface area up to 1148 $m^2 \cdot g^{-1}$ could be gained through combined physical and chemical activation,[9] demonstrating excellent performance in supercapacitors. Considering the similarities in the charge storage mechanism, it will be promising to explore their behaviours in LICs.

The wide application of LICs is limited by the relatively low energy density. To improve the performance of LICs, efforts have been made in the following two aspects. On the one hand, by shifting from acetonitrile- to carbonate- based electrolyte, a high working voltage with an oxidation potential up to 5 V vs. Li^+/Li can be obtained. On the other hand, in order to boost the capacity of the carbon cathode, numerous methods including heteroatom doping, catalysts-assisted growth and use of high surface area porous carbon have been applied.[1,10-13] In this work, a carbon material with an ultra-high surface area of over 2800 $m^2 \cdot g^{-1}$ is prepared using low-cost and bio-renewable lignin

[a] *Department of Applied Physics, the Hong Kong Polytechnic University, Hung Hom, Hong Kong, P.R. China;*
[b] *The Hong Kong Polytechnic University Shenzhen Research Institute, Shenzhen, P.R. China.*
Corresponding author: Biao Zhang. Email: biao.ap.zhang@polyu.edu.hk
† Footnotes relating to the title and/or authors should appear here.
Electronic Supplementary Information (ESI) available: [details of any supplementary information available should be included here]. See DOI: 10.1039/x0xx00000x

as the precursor. To fully explore its charge storage capability, a wide voltage window of 1.0-4.8 V is used and synergistic storage of anions and cations is unveiled. It is found that the anion storage in carbon materials is underestimated previously due to the incomplete desorption of shallow discharge. Furthermore, to combat the concerns on the limited lithium reserves,[14] the Na-ion capacitors (NICs) and K- ion capacitors (KICs) are also investigated using the same carbon cathode.

2. Results and discussion

In general, lignin was firstly carbonized at 600 °C (denoted as LC-600), and then activated by KOH at 900 °C (Fig. 1. *Route a*). After carbonization, the LC-600 shows a spherical shape with numerous macropores in the cross-section of the spheres (Fig. 2a). High magnification image in Fig. S1a shows that a great number of particles are coated on both the inner and outer surface of carbon spheres, which mainly consist of Na_2CO_3 as determined by XRD (Fig. 2d). The Na element originates from the lignin precursor, which is transferred into Na_2CO_3 during carbonization. After activation by KOH at 900 °C, the as-prepared carbon (LAC-900) maintains the spherical shape with a diameter ranging from 10~100 μm (Fig. 2c, S1d). LAC-800 and LAC-1000 were also prepared by activating at 800 °C and 1000 °C, respectively, they present the same morphology as LAC-900 (Fig. S1c, e). The XRD patterns (Fig. S2a) of LAC-800, -900 and -1000 share the same broad peak, indicating the low-graphitization degree of the activated carbon. As shown in Raman spectra (Fig. S2b), the D- and G-band appear at around 1340 cm^{-1} and 1586 cm^{-1} with an I_d/I_g ratio of 0.98, 1.02 and 1.07 for LAC-800, -900 and -1000, respectively. This further confirms the partly disordered state of the final activated carbon. The N_2 adsorption-desorption curves in Fig. S2c can be assigned to type I isotherms featuring activated carbon.[15] The BET parameters for all the samples are listed in Table S1, wherein a high surface area of 2321, 2880 and 3080 $m^2 \cdot g^{-1}$ is obtained for LAC-800, LAC-900 and LAC-1000, respectively, with the majority of pores located at 1.2 and 2.2 nm (Fig. S2d). It is worth noting that the surface areas of LAC-900 and LAC-1000 are among the highest values ever reported for KOH activated carbon materials.

To figure out the mechanism behind such high surface area, a comparative experiment was carried out following fabrication *route b* in Fig. 1, in which Na_2CO_3 impurity particles were deliberately removed after carbonization by washing in diluted HCl solution (7%) and DI water. The product is marked as LCw-600. XRD patterns and SEM images of LCw-600 in Fig. 2 and S1

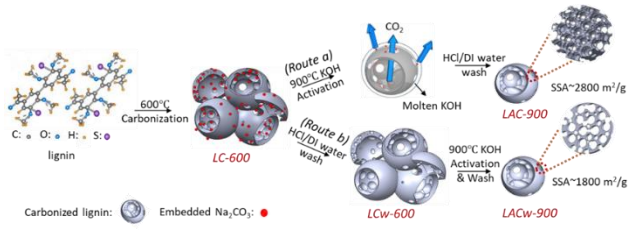

Fig. 1 Illustration of the fabrication process of activated carbon from lignin following two separate routes: route a and route b.

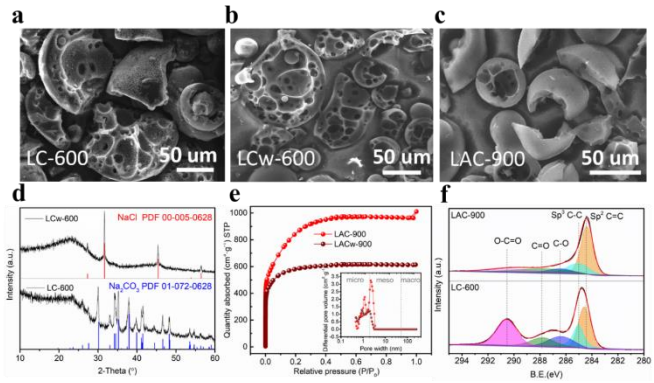

Fig. 2 Materials characterization. SEM images of a) LC-600 b) LCw-600 c) LAC-900; (d) XRD patterns of the samples after carbonization at 600 oC; (e) N_2 adsorption/desorption with the pore size distribution (inset); (f) XPS spectra of LAC-900 and LC-600.

verify the successful elimination of most of the impurity particles. The activation was then conducted identically to the preparation of LAC-900. Nonetheless, the final product (LACw-900) delivers a much lower surface area of 1829 $m^2 \cdot g^{-1}$ and a limited pore volume of 0.95 $cm^3 \cdot g^{-1}$ (Fig. 2e) with similar morphology compared to LAC-900. This observation emphasizes the important role of Na_2CO_3 that serves as a self-activation agent besides KOH etching. Although Na_2CO_3 was normally considered as an inactive agent for pore development due to its thermal stability during annealing.[16] It is demonstrated here Na_2CO_3 could be effective under high-temperature activation since the decomposition of Na_2CO_3 at around 900 °C[17] results in the generation of CO_2 gas whose escape leaves pores on the surface. The surface chemistry of the products is further analysed by XPS. Plenty of oxygenated functional groups, including carboxyl (O-C=O), carbonyl (C=O) and hydroxyl (C-O), are presented on the carbon surface of LC-600 (Fig. 2f). These groups together give a total oxygen content of 32 at. % (Table S2). High-temperature activation also greatly enhances the carbonization process through the growth of aromatic structure and elimination of heteroatoms,[18] resulting in a 96~98 at. % carbon amount and a merely 4~2 at. % oxygen for LAC-800, LAC-900 and LAC-1000, separately (Fig. S3 and Table S2, S3). Removal of the oxygenated functional groups is helpful to the conductivity for fast charge transfer. The sp^2 (C=C) structure content of LAC-900 is greatly improved to 53% while a high amount of sp^3 (C-C) structure remains since the annealing temperature is not high enough to fully graphitize the carbon materials.

The charge storage behaviours of the prepared carbon were evaluated in LICs with lithium metal as the counter electrode. The cells were firstly charged to stimulate the adsorption of anions (PF_6^-) in the electrolyte. A cut-off voltage of 4.8 V, which almost approaches the oxidation window of the electrolyte,[19] was applied to fully explore the anion storage capability. Within the voltage window of 1.0-4.8 V, LAC-800, LAC-900 and LAC-1000 are able to deliver a discharge capacity of 208, 326 and 302 $mAh \cdot g^{-1}$ at 2nd cycle at 0.1 $A \cdot g^{-1}$ (Fig. S4a) and demonstrate decent cycling performance (Fig. S4b). A 24% increase in the surface area is observed when the activation temperature rises from 800 °C to 900 °C, accounting for the large improvement in

the capacity. Further increase in the activation temperature does not affect much the performance due to the marginal amelioration on the surface area. The slightly lower capacity of LAC-1000 than LAC-900 may arise from the differences in pore size distributions, where the latter has larger micropore volume facilitating the anion adsorption. The dependence of capacity on the surface area is also confirmed by the performance of LACw-900, which shows a much lower capacity than LAC-900 due to reduced surface areas arising from the removal of Na_2CO_3 before activation (Fig. S4c).

Hence, the subsequent research aiming at uncovering the ion storage mechanisms is focused on LAC-900, of which the electrochemical performance proves optimum among all. As shown in Fig. 3a, it displays a promising first charge capacity of 186 mAh·g^{-1} thanks to the high surface area of carbon cathode. Upon discharge, the PF_6^- ions leave the carbon surface. It is noted that an equal capacity to the charge value is gained when discharged to around 1.8 V. Deep discharging also triggers the insertion of Li^+ cation, contributing to an accumulative capacity of 350 mAh·g^{-1} at 1.0 V. This capacity is among the highest value obtained in the carbon cathode for LICs so far and is largely maintained in the following cycles as shown in Fig. 3b. The phenomenon may not be attractive at first sight owing to the low discharge voltage of 1.0 V. The high capacity could be simply ascribed to the contribution from Li^+ ions insertion at low voltage, which normally occurs at a voltage lower than 3.0 V in carbon materials.[20] Therefore, the capacity contribution from cation is clarified by limiting the voltage range to 1.0-3.0 V. It shows an initial capacity of ~ 86 mAh·g^{-1} but quickly drops to no more than 20 mAh·g^{-1} occupying less than 10% of the total capacity. Interestingly, the cell also delivers a low capacity of around 75 mAh·g^{-1} when cycled between 3.0-4.8 V, which may result from the incomplete desorption of anions arising from early termination of discharging, as shown in Fig. 3b. This observation suggests a synergistic effect of both cation insertion and anion desorption involved between 1.0 and 3.0 V.

To further understand the effect of cation insertion, it necessitates the de-coupling of anion and cation storage. Therefore, we gradually open the electrochemical window by decreasing the end-of-discharge voltage from 3.0 to 1.0 V while the end-of-charge voltage is kept at 4.8 V, as shown in Fig. 3c. The cell was firstly activated by charging to 4.8 V. The state at this point, which indicates the full adsorption of PF_6^-, is used as a reference. All the curves are shifted so that they will overlap at 4.8 V to eliminate the capacity contribution from electrolyte decomposition. As expected, the discharge capacity continues to increase from 100 mAh·g^{-1} at an end-of-discharge potential of 3.0 V to 125 mAh·g^{-1} at 2.5 V, 167 mAh·g^{-1} at 2.0 V, 220 mAh·g^{-1} at 1.5 V and 318 mAh·g^{-1} at 1.0 V. It is surprising that a huge capacity of around 100 mAh·g^{-1} is gained between 1.5-1.0 V. The contribution from the Li^+ ion insertion alone cannot explain the remarkable capacity gain since the direct cycling between 1.0 and 3.0 V fails to show a considerable capacity. It may be argued that solid electrolyte interphase generation would occur at around 1.0 V, which would be partly responsible for the capacity increase. The contribution should not be such significant as demonstrated by the small irreversible capacity and good overlapping of voltage profiles in the following cycles (Fig. 3a). It suggests that the desorption potential of PF_6^- could be as low as 1.0 V, although the adsorption of anions takes place at a high potential up to 4.8 V. To support this finding, we probed the elemental composition of the electrodes at various

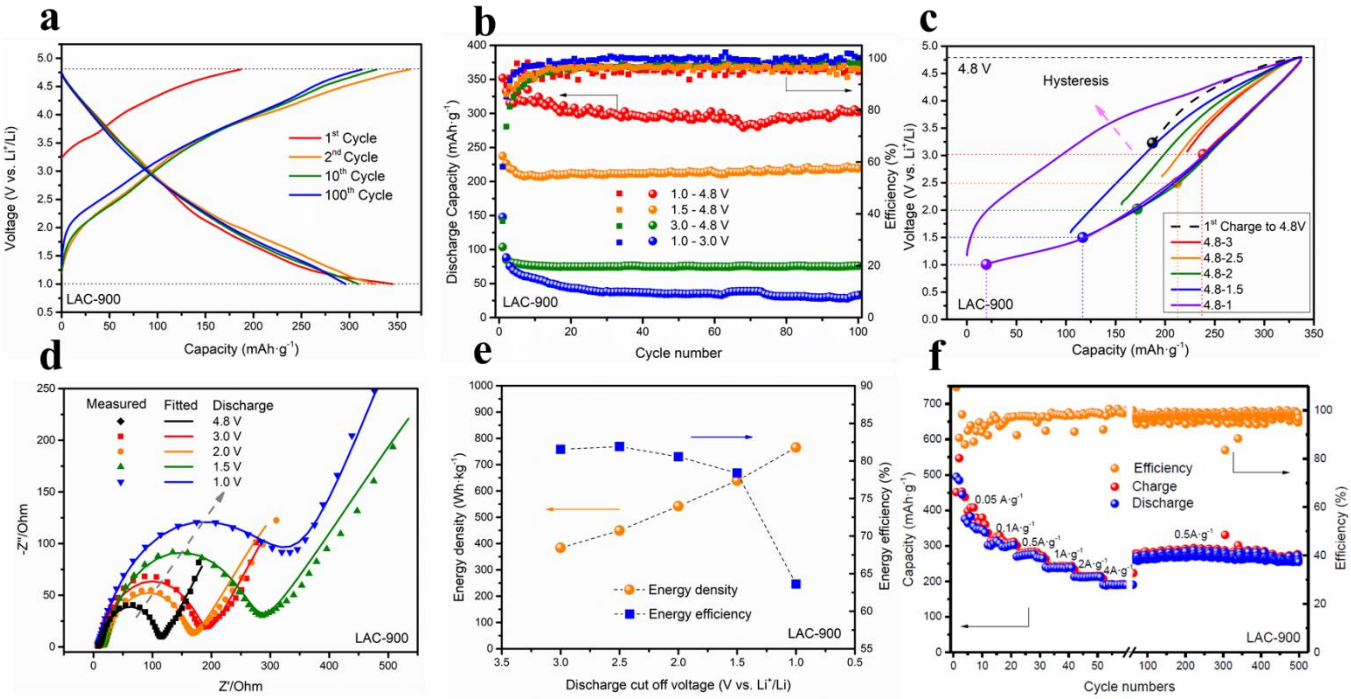

Fig. 3 Electrochemical performance of LICs with LAC-900 as the cathode material. (a) Voltage profiles; (b) Cyclic tests under various voltage range; (c) Voltage hysteresis and (d) Electrochemical impedance spectra of the LAC-900 electrode upon various discharge depth; (e) Energy density against energy efficiency with increasingly deep discharging; (f) Rate capability and long-term stability test.

charge/discharge depths by energy dispersive spectroscopy (EDS). Fig. S5 shows a continuous decrease of P and F content when discharging to 1.0 V, indicating the desorption of PF_6^- occurs in the whole discharge process. Therefore, the anion storage capability of carbon cathode is highly underestimated previously due to the early termination of discharge, resulting in partial desorption of adsorbed anions.

The voltage profiles in Fig. 3c show that although the energy density could be largely improved by deep discharge, the voltage hysteresis is also magnified, leading to low energy efficiency. The reason lies in the higher charge transfer resistance (R_{ct}) when discharging to a lower potential, as shown in Fig. 3d. A surge of R_{ct} from 112 Ω at 4.8 V to 182 Ω at 3.0 V and further to 330 Ω at 1.0 V has been observed (See more details in supporting information Fig. S6 and Table S4). The slight decrease of Rct from 3.0 to 2.0 V may due to the transition from anion adsorption to cation insertion with the complex process involved. The interplay between the anion and cation storage remains unclear and requires further exploration. Accordingly, the energy efficiency continues to decline when lowering the discharge cut-off voltage as shown in Fig. 3e. Note that the energy density shown here is based solely on the mass of carbon cathode to reflect the contributions from both the capacity and average voltage. Thus, a compromise must be made between energy density and efficiency depending on the application requirements. It is worth mentioning that despite the decreased energy efficiency upon deep discharge, the cyclability of the capacitor maintains excellent. A high capacity retention of 97% is achieved after cycling at 0.5 $A{\cdot}g^{-1}$ for 500 cycles (Fig. 3f). The cell also presents a decent rate capability with a capacity of 190 $mAh{\cdot}g^{-1}$ at 4.0 $A{\cdot}g^{-1}$ arising from the fast kinetics of capacitive behaviour.[21-23]

Na- and K- ion technologies have been revived recently due to the concern on the depletion of Li reserves.[24,25] Thus, we extend the application of the high surface carbon to Na and K ion capacitors (See details in experiment part of supporting information). Again, the discharge voltage window is gradually open to allow the entire desorption of anions. A similar phenomenon is observed that deep discharging increases the capacity and energy density but gives rise to the intensified polarization and energy efficiency loss as indicated by the large hysteresis (Fig. 4a, b and c). A promising capacity of 240 and 280 $mAh{\cdot}g^{-1}$ (Fig. 4d) is obtained at the second cycle with an average potential of 2.40 and 2.42 V for NICs and KICs, respectively, corresponding to an attractive energy density of 577 and 678 $Wh{\cdot}kg^{-1}$ (based on the mass of cathode). These values are comparable to the polyanionic and layered cathode in Na- and K- ion batteries.[26] Satisfactory capacity retention is obtained after 100 cycles. In comparison with LICs, both NICs and KICs exhibit relatively lower capacities by around 30% at the 50th cycle, the values of which are 220 and 215 $mAh{\cdot}g^{-1}$, respectively.

In-situ Raman tests were conducted to explore the origin of capacity discrepancies in the alkali-metal ion capacitors. Fig. 5a presents the Raman spectra in LICs for the carbon at various states. It can be seen that the D-band does not show a clear change in the whole charge/discharge processes. On the opposite, an up-shift of G-band is observed upon charging to 4.8 V, which is recovered once discharging to 3.0 V. The phenomenon reminds of the anion insertion in carbon materials at the high potential that is well understood in dual-ion batteries.[27] It is speculated that part of PF_6^- is intercalated into the cathode in additional to adsorption. Deep discharging to 1.0 V leads to a slightly down-shift of G-band due to the insertion of Li^+ ions. The position of the peak is fully restored in the subsequent charging to 3.0 V. The results confirm again the excellent reversibility of as-prepared carbon under the wide voltage range. In contrast to LICs, neither D- nor G- band of carbon in NICs and KICs (Fig. S7) undergoes distinct change under all the oxidation/reduction depths, arising from adsorption-governed behaviors.[28] Based on the above discussion, both diffusional and capacitive processes are involved in the alkali-metal ion capacitors. To quantify their individual contribution, current separation method was employed (Fig. S8 and S9).[29] At a scan rate of 2.0 $mV{\cdot}s^{-1}$, the capacitive contribution makes up 56.5%, 77.9%, and 76.3% of the total capacity in LICs, NICs and KICs (Fig. 5b), respectively. It suggests that a considerable capacity arises from insertion behaviour in LICs compared to adsorption/desorption-dominant behaviour in NICs and KICs, in agreement well with in-situ Raman results. The unfavourable insertion process in NICs and KICs gives rise to the lower capacity than LICs. The disparities in charge storage mechanism may originate from the

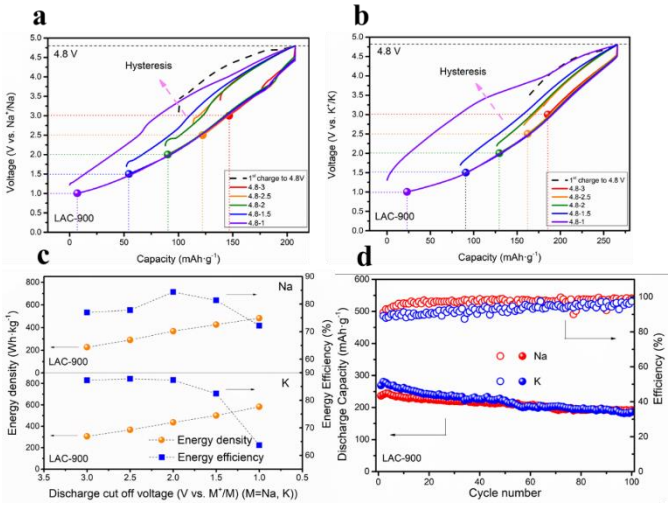

Fig. 4 Electrochemical performance in NICs and KICs with LAC-900 as a cathode. Voltage profiles for (a) NICs and (b) KICs; (c) Evolution of energy density and energy efficiency under the various electrochemical window; (d) cyclic stability of NICs and KICs.

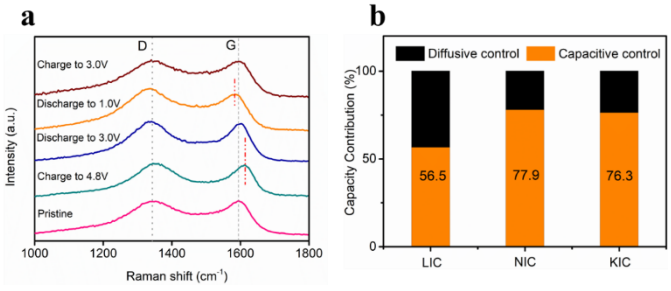

Fig. 5 Charge storage mechanism. (a) In-situ Raman of carbon cathode in LICs; (b) Capacity contribution of diffusive and capacitive behaviour in LICs, NICs and KICs.

solvation energy differences of the salts in the electrolytes and the corresponding electrode/electrolyte interphase in the three-type alkali-metal ion capacitors.[30] This information is little understood in the emerging Na- and K- ion systems, which requires further studies in order to catch up with the performance in LICs. Lastly, it should be mentioned that the co-utilization of anion and cation storage in the cathode might bring difficulty in the practical application, as the pre-loading of cations (Li, Na, K) in the carbon is demanded. Fortunately, this issue would be overcome by the utilization of alkali-metal anode, a topic that is intensively exploring in the battery community.[31]

3. Conclusions

It shows here the lignin-derived activated carbon are promising cathodes in LICs. Two strategies are adopted to achieve an attractive energy density, including i) utilizing the self-activation from the Na_2CO_3 impurities for obtaining exceptional surface area; and ii) performing deep discharging to allow the full desorption of PF_6^- anions. A synergistic effect of cation insertion and anion adsorption is revealed. Both the capacity and energy density are remarkably enhanced when decreasing the discharge-end voltage to 1.0 V, accompanying with the increased voltage hysteresis and the corresponding low energy efficiency. Similar phenomenon is observed in both NICs and KICs. Therefore, for practical applications, a trade-off needs to be made via adopting a suitable voltage window.

Conflicts of interest

There are no conflicts to declare.

Acknowledgments

This work was financially supported by the Hong Kong Polytechnic University (Grant 1-ZE83), the Innovation and Technology Commission (ITF Project ITS/029/17) and the General Research Fund (25215918) of Hong Kong SAR, and the Key Project for Basic Research of Shenzhen (No. JCYJ20170818104125570).

References

1 J. Ding, W. Hu, E. Paek, D. Mitlin, Review of Hybrid Ion Capacitors: From Aqueous to Lithium to Sodium, *Chem*. *Rev*., 2018, **118**(14), 6457–6498.
2 A. Byeon, M. Boota, M. Beidaghi, K. V. Aken, J. W. Lee, Y. Gogotsi, Effect of Hydrogenation on Performance of TiO_2(B) Nanowire for Lithium Ion Capacitors, *Electrochem. commun*., 2015, **60**, 199–203.
3 E. Morall, D. Cazorla-amor, Asymmetric Capacitors Using Lignin-Based Hierarchical Porous Carbons, *J. Power Sources*, 2016, **326**, 641–651.
4 F. Wang, X. Wu, X. Yuan, Z. Liu, Y. Zhang, L. Fu, Y. Zhu, Q. Zhou, Y. Wu, W. Huang,Latest advances in supercapacitors: from new electrode materials to novel device designs. *Chem. Soc. Rev.*, 2017,**46**(22), 6816-6854.
5 F. Wang, C. Wang, Y. Zhao, Z. Liu, Z. Chang, L. Fu, Y. Zhu, Y. Wu, D. Zhao, A quasi-solid-state Li-ion capacitor based on porous TiO2 hollow microspheres wrapped with graphene nanosheets. *Small*, 2016, *12*(45), 6207-6213.
6 C. Han, H. Li, R. Shi, L. Xu, J. Li, F. Kang, B. Li, Nanostructured Anode Materials for Non-aqueous Lithium Ion Hybrid Capacitors, *Energy Environ. Mater*., 2018, **1**, 75–87.
7 G. Tang, L. Cao, P. Xiao, Y. Zhang, H. Liu, A novel high energy hybrid Li-ion capacitor with a three-dimensional hierarchical ternary nanostructure of hydrogen-treated TiO_2 nanoparticles/conductive polymer/carbon nanotubes anode and an activated carbon cathode, *J. Power Sources*, 2017, **355**, 1-7.
8 D. Salinas-Torres, R. Ruiz-Rosas, M. J. Valero-Romero, J. Rodríguez- Mirasol, T. Cordero, E. Morallon, D. Cazorla-Amoros, Asymmetric capacitors using lignin-based hierarchical porous carbons, *J. Power Sources*, 2017, **355**, 1-7.
9 D. Saha, Y. Li, Z. Bi, J. Chen, J. K. Keum, D. K. Hensley, H. A. Grappe, H. M. Meyer, S. Dai, M. P. Paranthaman, Studies on Supercapacitor Electrode Material from Activated Lignin-Derived Mesoporous Carbon, *Langmuir*, 2014, **30**, 900–910.
10 Q. Xia, H. Yang, M. Wang, M. Yang, Q. Guo, L. Wan, H. Xia, Y. Yu, High Energy and High Power Lithium-Ion Capacitors Based on Boron and Nitrogen Dual-Doped 3D Carbon Nanofibers as Both Cathode and Anode, *Adv. Energy Mater*., 2017, **7**(22), 1–9.
11 R. V. Salvatierra, D. Zakhidov, J. Sha, N. D. Kim, S. K. Lee, A. R. O. Raji, N. Zhao, J. M. Tour, Graphene Carbon Nanotube Carpets Grown Using Binary Catalysts for High-Performance Lithium-Ion Capacitors, *ACS Nano*, 2017, **11**(3), 2724–2733.
12 D. Puthusseri, V. Aravindan, S. Madhavi, S. Ogale, Improving the Energy Density of Li-Ion Capacitors Using Polymer-Derived Porous Carbons as Cathode, *Electrochim. Acta*, 2014, **130**, 766–770.
13 Y. Zhang, H. Feng, X. Wu, L. Wang, A. Zhang, T. Xia, H. Dong, X. Li, L. Zhang, Progress of Electrochemical Capacitor Electrode Materials: A Review, *Int. J. Hydrogen Energy*, 2009, **34**(11), 4889–4899.
14 D. Larcher, J. Tarascon, Towards Greener and More Sustainable Batteries for Electrical Energy Storage, *Nat. Chem*, 2014, **7**(1), 19–29.
15 Kenneth SW. Sing, Reporting physisorption data for gas/solid systems with special reference to the determination of surface area and porosity (Recommendations 1984), *Pure and applied chemistry*, 1985, **57**(4), 603-619.
16 M. Rodenas, D. Amoros, A. Solano, Understanding Chemical Reactions between Carbons and NaOH and KOH An Insight into the Chemical Activation Mechanism, *Carbon*, 2003, **41**, 267–275.
17 K. Motzfeldt, The Thermal Decomposition of Sodium Carbonate by the Effusion Method, *J. Phys. Chem*., 1955, **59**, 139–147.
18 B. Zhang, C. M. Ghimbeu, C. Laberty, C. Vix-Guterl, J. M. Tarascon, Correlation Between Microstructure and Na Storage Behavior in Hard Carbon, *Adv. Energy Mater*., 2016, **6**(1), 1–9.
19 K. Xu, Electrolytes and Interphases in Li-Ion Batteries and Beyond, *Chemical reviews*, 2014, **114**(23), 11503-11618.
20 J. R. Dahn, T. Zheng, Y. Liu, J. S. Xue, Mechanisms for lithium insertion in carbonaceous materials, *Science*, 1995, **270**, 590-593.
21 Y Tang, J Deng, W Li,O. I. Malyi, Y. Zhang, X. Zhou, S. Pan, J. Wei, Y. Cai, Z. Chen, X. Chen, Water‐Soluble Sericin Protein Enabling Stable Solid–Electrolyte Interphase for Fast Charging High Voltage Battery Electrode. *Adv. Mater.*, 2017, **29**(33), 1701828.

22 Y Tang, Y Zhang, O.I. Malyi, N. Bucher, H. Xia, S. Xi, Z. Zhu, Z. Lv, W. Li, J. Wei, M. Srinivasan, A. Borgna, M. Antonietti, Y. Du, X. Chen,Identifying the origin and contribution of surface storage in TiO2(B) nanotube electrode by in situ dynamic valence state monitoring. *Adv. Mater.*, 2018, **30**(33), 1802200.

23 Y. Zhang, O. I. Malyi, Y. Tang, J. Wei, Z. Zhu, H. Xia, W. Li, J. Guo, X. Zhou, Z. Chen, C. Persson, X. Chen, Reducing the Charge Carrier Transport Barrier in Functionally Layer‐Graded Electrodes. *Angew. Chem. Int. Ed.* 2017, **56**, 14847.

24 J. Ding, H. Wang, Z. Li, K. Cui, D. Karpuzov, X. Tan, A. Kohandehghan, D. Mitlin, Peanut Shell Hybrid Sodium Ion Capacitor with Extreme Energy – Power Rivals Lithium Ion Capacitors †, *Energy Environ. Sci*., 2015, **8**(3), 941–955.

25 A. Le Comte, Y. Reynier, C. Vincens, C. Leys, P. Azaïs, First Prototypes of Hybrid Potassium-Ion Capacitor (KIC): An Innovative, Cost-Effective Energy Storage Technology for Transportation Applications, *J. Power Sources*, 2017, **363**, 34–43.

26 X. Lin, J. Huang, H. Tan, J. Huang, B. Zhang, $K_3V_2(PO_4)_2F_3$ as a Robust Cathode for Potassium-Ion Batteries, *Energy Storage Mater*., 2019, **16**, 97–101.

27 B. Ji, F. Zhang, X. Song, Y. Tang, A Novel Potassium-Ion-Based Dual-Ion Battery, *Adv. Mater*., 2017, **29**, 1700519.

28 X. Lin, J. Huang, B. Zhang, Correlation between the Microstructure of Carbon Materials and Their Potassium Ion Storage Performance, *Carbon*, 2019, **143**, 138–146.

29 J. Wang, J. Polleux, J. Lim, B. Dunn, Pseudocapacitive Contributions to Electrochemical Energy Storage in TiO_2(Anatase) Nanoparticles, *J. Phys. Chem. C*, 2007, **111**(40), 14925–14931.

30 M. Okoshi, Y. Yamada, S. Komaba, A. Yamada, Theoretical Analysis of Interactions between Potassium Ions and Organic Electrolyte Solvents: A Comparison with Lithium, Sodium, and Magnesium Ions, *J. Electrochem. Soc*., 2017, **164**(2), 54–60.

31 Y. Gu, W. Wang, Y. Li, Q. Wu, S. Tang, J. Yan, M. Zheng, D. Wu, C. Fan, W. Hu, Designable Ultra-Smooth Ultra-Thin Solid-Electrolyte Interphases of Three Alkali Metal Anodes, *Nature Commun*., 2018, **9**, 1339.